HHS Public Access

Author manuscript

Kidney Int. Author manuscript; available in PMC 2020 December 01.

Published in final edited form as:

Kidney Int. 2019 December ; 96(6): 1332–1345. doi:10.1016/j.kint.2019.07.017.

miR-146b-5p has a sex-specific role in renal and cardiac pathology in a rat model of chronic kidney disease.

Mark R. Paterson[1], **Aron M. Geurts**[1,2,3], **Alison J. Kriegel**[1,3]

[1]Department of Physiology, Medical College of Wisconsin, Milwaukee, WI

[2]Genomics Sciences and Precision Medicine Center, Medical College of Wisconsin, Milwaukee, WI

[3]Center of Systems Molecular Medicine, Medical College of Wisconsin, Milwaukee, WI

Abstract

Chronic kidney disease presents a complex and distinct pathological landscape in men and women, yet this difference is poorly understood. microRNAs are powerful molecular regulators of pathophysiology in the kidney and other organs. We previously reported a significant upregulation of miR-146b-5p in the 5/6 nephrectomy rat model of chronic kidney disease. Here we investigated the sex-specific contribution of miR-146b-5p to renocardiac pathology by generating a novel miR-146b$^{-/-}$ rat and characterized the expression of miR-146b-5p in both wild-type and knockout animals. The 5/6 nephrectomy or sham surgery was performed on rats of each genotype and sex. Renal pathology was examined through gross histology, plasma and urinary analysis of electrolytes and metabolites, and by chronic blood pressure monitoring. Cardiac pathology was monitored via echocardiography and pressure-volume analysis. The miR-146b$^{-/-}$ rats show functional knockout of miR-146b-5p in both the kidney and heart. While 5/6 nephrectomy induced tissue hypertrophy, miR-146b$^{-/-}$ female rats displayed exacerbated renal hypertrophy. Additionally, miR-146b$^{-/-}$ female rats exhibited a marked elevation of renal fibrosis and significant renal dysfunction yet lower blood pressure and less pronounced cardiac remodeling. These phenotypic differences were not exhibited in miR-146b$^{-/-}$ male rats. Ovariectomy ameliorated renal pathology and abolished genotypic differences. *In vitro* examination of transforming growth factor-β signaling in combination with miR-146b-5p manipulation supports a role for miR-146b-5p in mediating the protective benefit of estrogen from renal pathologies. Thus,

Correspondence: Alison J. Kriegel, PhD, FAHA, Department of Physiology, Medical College of Wisconsin, 8701 Watertown Plank Rd., Milwaukee, WI 53226, Phone: 414-955-4835, Fax: 414-955-6456, akriegel@mcw.edu.

AUTHOR CONTRIBUTIONS

M.R.P. and A.J.K. designed the study; A.M.G. provided the null mutant rat model; M.R.P. and A.J.K. carried out experiments; M.R.P. and A.J.K. analyzed the data; M.R.P. made the figures; M.R.P. drafted the manuscript; M.R.P. and A.J.K. revised the manuscript; all authors approved the final version of the manuscript.

DISCLOSURES

None.

Supplementary information is available at Kidney International's website.

our data highlight an important role of miR-146b-5p in modulating kidney disease progression and provide new avenues for the study of sex-specific pathology

Graphical Abstract

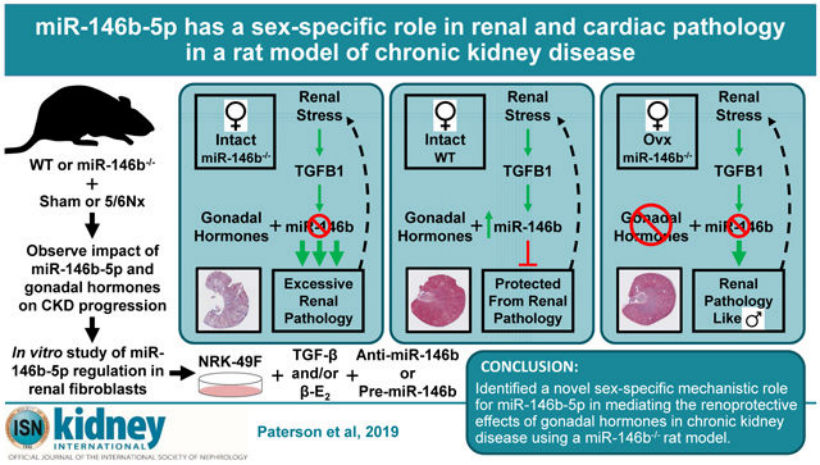

Keywords

microRNA; CKD; kidney; heart; sex differences

INTRODUCTION

Cardiorenal syndrome type 4 (CRS4) is a well-defined clinical condition in which primary chronic kidney disease (CKD) contributes to secondary cardiovascular impairment (CVD). Awareness of CRS4 in a clinical setting has grown in recent years due, in part, to the staggering domestic and international healthcare burden of CKD. Estimates suggest over 15% of the adult US population has CKD, with an equally stunning global prevalence.[1, 2] CVD and cardiovascular events are the leading cause of death among CKD patients and CVD-related mortality increases dramatically with progressive CKD.[3] CVD manifests differently in the presence of CKD, an independent risk factor for CVD, and risk persists despite advanced renal therapies.[4]

Compounding these challenges, a large body of literature supports marked differences in etiology, progression, and outcomes of CKD between men and women.[5, 6] Men are more likely to progress to end-stage renal disease and have higher incidence of CKD-related CVD than women. However, women have a higher age-adjusted prevalence of CKD.[7] Pre-menopausal women are generally considered to be protected from the development of CKD and CVD due to the protective benefit of gonadal hormones, and hormone replacement therapy has long been a trending topic in CKD management in post-menopausal women.[8, 9] These studies emphasize the important role of gonadal hormones and highlight a need to understand poorly-defined sex-specific signaling mechanisms.

We have focused on identifying novel microRNA (miRNA) signaling pathways that contribute to CKD utilizing a well-characterized remnant kidney model of CKD – the 5/6 nephrectomy excision model (5/6Nx). miRNAs are a class of small, non-coding RNAs that exert a biological effect by suppressing the translation of target mRNA transcripts, thus reducing target protein expression.[10] We recently reported significant alterations of left ventricular (LV) miRNA expression profiles in male Sprague-Dawley (SD) rats following 5/6Nx.[11] Growing evidence indicates that miRNAs, including miR-146b-5p, are important mediators of renocardiac pathophysiology.[11] Increased miR-146b-5p abundance has been reported in clinical studies of renal pathology and experimental disease models; including hypertension, AKI, renal fibrosis, and CKD.[12-15]

We generated a novel miR-146b-5p specific null mutant rat (miR-146b$^{-/-}$), allowing us to definitively dissect biological effects of miR-146b apart from that of its miR-family member miR-146a.[16] We have identified a unique sex-specific protective role for miR-146b-5p in CKD pathology. Given the important clinical divergence of CKD-mediated pathologies in men and women, our findings reinforce the need to explore the implications of molecular changes which drive sex-specific responses in CKD.

RESULTS

Mutagenesis of *Mir146b* and tissue expression of *Mir146b* gene products

We utilized CRISPR-Cas9 technology to induce germline mutation of *Mir146b* and produce a novel miR-146b-5p global knockout animal. CRISPR guide RNAs were designed to direct the SpCas9 nuclease to cleave within the seed sequence of the mature miR-146b-5p (Figure 1A). Cleavage of the gene resulted in a 7-bp deletion mutation in the intended this region (Figure 1B, bottom). In order to fully characterize *Mir146b* expression in our model, we measured the primary transcript (Figure 1D; pri-miR-146b), the intermediate precursor (Figure 1E; pre-miR-146b), and the mature guide strand (Figure 1F; miR-146b-5p) by qRT-PCR in miR-146b$^{-/-}$ and wild-type (WT) rats. The genetic manipulation of the *Mir146b* locus did not prevent expression of pri-miR-146b (Figure 1D) or pre-miR-146b (Figure 1E). miR-146b-5p abundance increases with 5/6Nx in kidney and LV and is completely abolished in miR-146b$^{-/-}$ (Figure 1F). There is no difference in the basal expression of miR-146b-5p between sexes (Figure 1C). We used *in situ* hybridization (ISH) to visualize expression of miR-146b-5p. Representative images of WT sham, WT 5/6Nx, and miR-146b$^{-/-}$ 5/6Nx kidneys show that miR-146b-5p expression in the sham is localized to the cortical distal tubules with little to no expression in the medulla (Supplementary Figure S1). Conversely, following 5/6Nx, cortical expression of miR-146b-5p is localized to the parietal layer of Bowman's capsule, proximal tubular epithelial cells, and interstitial cells (Figure 1; Supplementary Figure S1). In the heart, increased miR-146b-5p expression is detected throughout the myocardium and vasculature. These data confirm a viable miR-146b$^{-/-}$ rat model to study the contribution of miR-146b-5p to renocardiac pathologies.

Attenuated weight gain and increased urinary output following 5/6Nx

All experimental groups were followed for 7 weeks post-surgery to examine the pathophysiological changes in both the kidney and the heart along with gross phenotypic

changes. A slight attenuation of weight gain was observed 7 weeks after 5/6Nx in both males (Figure 2A; top) and females (Figure 2A; bottom). Urinary output (24h) was significantly increased in 5/6Nx males throughout the 7-week study (Figure 2B; top). Females did not exhibit a consistent increase in 24h urinary output after 5/6Nx. However, the miR-146b$^{-/-}$ 5/6Nx females tended to produce more urine than sham, with a notable increase at 5 weeks post-5/6Nx (Figure 2B; bottom).

Sex-specific tissue hypertrophy in miR-146b$^{-/-}$ rats

Renal and cardiac hypertrophy are classic pathological changes associated with the 5/6Nx model of CKD. WT males and females exhibited significant renal and cardiac hypertrophy after 5/6Nx. The loss of miR-146b-5p had no effect on the hypertrophic response in males. However, miR-146b$^{-/-}$ females tended to develop more pronounced renal hypertrophy and less pronounced cardiac hypertrophy following 5/6Nx compared to WT. (Figures 2C & 2D).

Histological and transcript-level examination of sex-specific renal fibrosis

Representative images of kidney pathology in male and female rats are shown (Figure 3A) with corresponding quantification of fibrotic area (Figure 3B). Whole kidney cross-sections are shown in Supplementary Figure S2. Qualitative examination of kidney sections in males revealed similar tubular damage and glomerular hypertrophy with no significant fibrosis following 5/6Nx[11] with no differences between WT and miR-146b$^{-/-}$ (Figure 3A & 3B; top). We observed exacerbated renal pathology following 5/6Nx in miR-146b$^{-/-}$ females but not in WT; this included severe glomerular damage and tubular dilation (Figure 3A; bottom), and increased renal fibrosis (Figure 3B; bottom). Transcript abundance of genes associated with fibrosis, including collagen family members *Col1a1*, *Col3a1*, and *Col4a1*; α-smooth muscle actin (*Acta2*); and fibronectin (*Fn1*) were analyzed by qRT-PCR. *Col1a1*, *Col3a1*, and *Fn1* were overexpressed following 5/6Nx while *Col4a1* and *Acta2* remained unchanged following 5/6Nx, regardless of genotype (Figure 3C). To determine if global knockout of miR-146b-5p elicited a broad fibrotic phenotype, we examined Masson's trichrome stained liver tissues. We observed no overt signs of fibrosis in the liver across all groups (Supplementary Figure S3).

Pronounced renal dysfunction in miR-146b$^{-/-}$ females

Plasma creatinine, creatinine clearance (CrCl), fractional excretion of sodium (FE_{Na}), and urinary microalbumin excretion ($U_{malb}V$) were analyzed as indices of renal function 7 weeks post-surgery. Males, regardless of genotype, exhibit a modest rise in plasma creatinine (Figure 4A; top), a drop in CrCl (Figure 4B; top), and a mild increase in FE_{Na} (Figure 4C; top). miR-146b$^{-/-}$ males exhibited a significant increase in $U_{malb}V$ following 5/6Nx compared to miR-146b$^{-/-}$ sham, but not compared to WT (Figure 4D; top). miR-146b$^{-/-}$ females exhibit increased plasma creatinine compared to WT controls (Figure 4A; bottom) and sharply reduced CrCl (Figure 4B; bottom), suggesting severely reduced renal filtration. FE_{Na} (Figure 4C; bottom) and $U_{malb}V$ (Figure 4D; bottom) in miR-146b$^{-/-}$ 5/6Nx females are significantly elevated compared to WT 5/6Nx.

Chronic blood pressure monitoring and cardiac remodeling

To understand the impact of renal dysfunction on the cardiovascular system, conscious mean arterial blood pressure (MAP), LV structure, and LV function were monitored throughout the study. Males develop a mild increase in MAP, regardless of genotype, between weeks 4 and 5 of the study (Figure 5A; top) with no change in developed pressure (P_{dev}; Figure 5B; top). Longitudinal echocardiography studies revealed gradual LV hypertrophy in WT 5/6Nx males (Figure 5C; top) concurrent with a steady dilation of the LV chamber (Figure 5D; bottom). Females exhibited a sex-specific exacerbation of the hypertensive phenotype, with WT 5/6Nx females the only group to exhibit a moderate to severe increase in MAP (Figure 5A; bottom). Interestingly, miR-146b$^{-/-}$ 5/6Nx females had no significant elevations in MAP. P_{dev} increased in WT females at 7 weeks following 5/6Nx, and this increase was ameliorated with miR-146b$^{-/-}$ (Figure 5B; bottom). WT females exhibited more pronounced cardiac remodeling compared to the miR-146b$^{-/-}$ females, with significant thickening of the ventral wall (Figure 5C; bottom) and LV chamber dilation (Figure 5D; bottom), corresponding to the sharp increase in MAP in WT 5/6Nx females. Representative images of LV pathology are shown (Figure 6A) with corresponding quantification of fibrotic area (Figure 6B). Males exhibit no development of cardiac fibrosis, regardless of genotype (Figure 6B; top). miR-146b$^{-/-}$ females tend to develop mild cardiac fibrosis (Figure 6B; bottom). Ejection fraction was unchanged at week 7 across all groups, suggesting a condition of preserved ejection fraction following 5/6Nx (Figure 6C). Likewise, arterial elastance, an index of vascular load, was unchanged across all groups (Figure 6D). While dP/dt_{max}, a measure of cardiac contractility, was unchanged in males (Figure 6E; top), WT females exhibited increased dP/dt_{max} following 5/6Nx compared to sham and miR-146b$^{-/-}$ (Figure 6E; bottom), which may correspond to the more pronounced cardiac remodeling observed in WT females. Taken together, miR-146b$^{-/-}$ females exhibit divergent cardiac phenotypes from males or WT females.

Ovariectomy attenuates renal phenotypes in miR-146b$^{-/-}$ females

With a clear sex-specific effect on renal and cardiac phenotypes in miR-146b$^{-/-}$ rats following 5/6Nx, we tested whether the gonadal status of the animal contributed to pathology. The increase in miR-146b-5p following 5/6Nx in WT females was attenuated by Ovx (Figure 7A). Ovx females exhibit increased weight gain across all groups (Figure 7B), a well-known effect of estrogen loss.[17] The exaggerated renal hypertrophy and fibrosis exhibited by hormonally-intact (intact) miR-146b$^{-/-}$ 5/6Nx females was significantly attenuated in Ovx (Figure 7C and 7D, respectively). While 5/6Nx still elicited cardiac hypertrophy regardless of genotype, the difference in the hypertrophic response between WT and miR-146b$^{-/-}$ and the development of LV fibrosis was abolished (Figure 7E and 7F, respectively). Acute arterial blood pressures in anesthetized females were not affected by Ovx (not shown). WT 5/6Nx Ovx females exhibit thickening of the LV wall by week 5, which is not seen in miR-146b$^{-/-}$ 5/6Nx Ovx females (Figure 7G; refer to Figure 5C, bottom). This wall thickening in Ovx females is not concurrent with significant chamber dilation as seen in intact females (Figure 7H; refer to Figure 4D, bottom). Further, renal dysfunction in miR-146b$^{-/-}$ females was ameliorated with Ovx. While 5/6Nx induced a significant elevation of plasma creatinine in Ovx females (Figure 7I), this increase was significantly attenuated compared to intact females. Likewise, CrCl and FE_{Na} were

significantly restored by Ovx (Figure 7J and 7K). The increase in $U_{malb}V$ following 5/6Nx was similar in miR-146b$^{-/-}$ Ovx and intact females (Figure 7L). These data suggest that renal function was significantly improved in miR-146b$^{-/-}$ Ovx females, and supports a role for miR-146b-5p in facilitating the effect of gonadal hormones in mediating CKD and its related pathologies.

Pathway analysis and markers of TGF-β signaling and the EMT pathway

In order to investigate potential mechanisms by which miR-146b-5p is modulating the observed pathological phenotypes, *in silico* analysis of all miR-146b-5p targets (reported by the TargetScan database[18]) was used to predict major pathways involved (Ingenuity Pathway Analysis, IPA; QIAGEN, Hilden, Germany). The transforming growth factor-β (TGF-β) signaling pathway was significantly represented (p = 3.27e-4) by predicted miR-146b-5p targets, which accounted for 25 of the 93 associated molecules. The canonical TGF-β signaling pathway is shown with nodes associated with predicted miR-146b-5p targets highlighted in orange (Figure 8A), displaying the potential of miR-146b-5p regulation at every level of TGF-β signaling. Moreover, examination of the IPA toxicity lists – those pathways and functions known to be linked to clinical pathologies – reveals TGF-β signaling to be one of the most significantly represented (−log[p-value] = 3.26) by miR-146b-5p targets (Figure 8B).

We examined the expression of TGFB1 protein and epithelial-to-mesenchymal transition (EMT) markers. 5/6Nx induced TGFB1 expression in all groups, regardless of sex or genotype (Figure 9A). EMT markers vimentin (*Vim*) and e-cadherin (*Cdh1*) represent the mesenchymal and epithelial phenotypes, respectively (Figure 9B and 9C). We observed increased abundance of *Vim* following 5/6Nx, regardless of sex or genotype. However, while males showed no changes in the abundance of *Cdh1*, miR-146b$^{-/-}$ females showed significantly reduced levels of *Cdh1* following 5/6Nx compared to WT and sham.

Manipulation of miR-146b, TGF-β, and β–estradiol in NRK-49F

Given the significant exacerbation of kidney pathology and increased fibrosis in the miR-146b$^{-/-}$ female, we examined the contribution of miR-146b, TGF-β, and β–estradiol (β–E_2) in normal rat kidney fibroblasts (NRK-49F) *in vitro*. Anti-miR-146b-5p treatment effectively knocked down the abundance of miR-146b-5p (Figure 10A). The abundance of *Vim* (Figure 10B) and *Fn1* (Figure 10D) were largely unchanged across treatment groups. While TGF-β increased abundance of *Col1a1* (Figure 10C), anti-miR-146b-5p did not significantly impact expression of this fibrosis marker. Pre-miR-146b treatment effectively increased the abundance of miR-146b-5p across all groups (Figure 11A). pre-miR-146b treatment reduced the abundance of *Vim*, the upregulation of which was driven by TGF-β treatment (Figure 11B). β–E_2 also tended to reduce the TGF-β-driven increase in *Vim* abundance (Figure 11B). pre-miR-146b treatment significantly reduced the abundance of *Col1a1* in TGF-β + β–E_2 treated cells but not TGF-β-treated cells alone (Figure 11C). While TGF-β treatment increased abundance of *Fn1*, with or without β–E_2, pre-miR-146b treatment significantly reduced *Fn1* abundance in both groups (Figure 11D).

DISCUSSION

A growing body of literature suggests that miR-146b-5p abundance is elevated in both clinical studies of renal pathology and experimental disease models. In this study, we have confirmed the upregulation of miR-146b-5p in both the kidney and the heart in a well-characterized model of CKD in the rat, providing a renal injury model that could be utilized to make a comparison between the pathological effects of 5/6Nx in the presence, and absence, of miR-146b-5p.

The findings of this study, taken together, indicate that miR-146b-5p modulates the pathogenesis of CKD in a sex specific manner. WT males and females exhibit similar pathological changes throughout the course of the 5/6Nx; changes which are within normal biological variance, with consideration of differences in strain, diet, and methodology in various experimental models.[19, 20] Exaggerated pathological changes occur in the absence of miR-146b-5p only in females, and are dependent on gonadal hormone status. miR-146b$^{-/-}$ females experience a significant exacerbation of kidney dysfunction compared to WT despite exhibiting normal blood pressure compared to hypertensive WT females. Hypertension is a classic impetus for pathological cardiac remodeling, and hypertensive kidney injury is widely-known and well-studied.[21] Out data suggest progression of advanced renal injury in miR-146b$^{-/-}$ females is independent of changes in arterial load and may be attributed to dysregulation at the molecular level. WT females experience significant elevations in chronic MAP, consequential hypertrophic cardiac remodeling, and moderate renal dysfunction. Conversely, miR-146b$^{-/-}$ females are virtually normotensive yet exhibit significantly worse renal injury.

The genotype effect is evidently connected to gonadal status, as Ovx abolishes the genotypic differences and largely restores renal function. While the protective effect of Ovx in miR-146b$^{-/-}$ females may be due to individual or combined effects of gonadal hormones, we suggest miR-146b-5p in the intact female may facilitate the protective effects of estrogen, and thus removal of negative suppression by miR-146b-5p (i.e. miR-146b$^{-/-}$) results in dysregulation of gonadal hormone signaling and exacerbation of CKD.

While women have slightly higher overall prevalence of all-stage CKD (age-adjusted) it is thought that men experience more rapid and severe CKD progression with worse overall outcomes.[6, 22] Age plays a major role in CKD outcomes in both men and women[23], but in females a direct link to hormonal status, i.e. pre- vs. post-menopausal, has been shown to be important in mediating renal function and the development of hypertension.[24] Likewise, estrogen is commonly regarded as conferring protection from renal disease.[25, 26] Estrogen affects the renin-angiotensin system and may be involved in the progression of CKD.[8] Moreover, estrogen replacement therapy and selective estrogen receptor modulation have been used, although still debated, as targeted therapeutics, especially post-menopause.[27] These studies highlight the important role of modulating estrogen signaling in the maintenance of kidney function.

Determining the target-specific effects of a single miRNA in a complex pathological landscape is daunting. A leading paradigm suggests miRNAs may exert their biological

function, in part, by silencing multiple targets in a single pathway thereby suppressing the effects of the whole cascade.[28] TGF-β signaling and EMT are two such pathways in which miR-146b-5p predicted targets are disproportionately represented by *in silico* pathway analysis (IPA; QIAGEN). These pathways have a direct cause-effect relationship – TGF-β stimulates EMT – but are also well-known contributors to renal pathology, especially renal fibrosis.[29, 30] *In silico* target analysis provided strong rationale to investigate the TGF-β signaling pathway and TGF-β-induced EMT. The pro-fibrotic and mitogenic effects of angiotensin-II (Ang-II) and endothelin (ET-1) act through TGF-β signaling.[31, 32] The expression pattern of fibrosis-related markers in the 5/6Nx kidneys (Figure 3C) does not sufficiently explain the exacerbated fibrosis exhibited by miR-146b$^{-/-}$ females following 5/6Nx, especially compared to the minimal fibrotic scarring exhibited by the other groups. This suggests a distinct mechanism impacted by miR-146b-5p in females. TGF-β plays an important role in the progression of CKD and induces EMT in the kidney.[30, 33] Although we show induction of TGF-β expression in all 5/6Nx rats, regardless of sex or genotype, we note that only the miR-146b$^{-/-}$ 5/6Nx females exhibit a loss of the epithelial marker *Cdh1* (Figure 8C). This suggests females, in the absence of miR-146b-5p, are sensitized to the EMT-inducing effects of TGF-β and experience a significant loss of renal epithelial cell-cell adhesion following 5/6Nx contributing to severe CKD progression. This sensitization appears to depend on the gonadal hormone status.

Identifying cell-specific effects of miR-146b-5p is essential to an understanding of this interplay between gonadal hormone signaling and miR-146b-5p activity. Given the striking increase in renal fibrosis and kidney dysfunction in 5/6Nx miR-146b$^{-/-}$ females, we examined the components of the proposed signaling pathways *in vitro* by manipulating miR-146b-5p, TGF-β, and β-E_2 in NRK-49F cells. Significantly reducing the abundance of miR-146b-5p had little to no effect on the expression pattern of these important markers of fibrosis (Figure 10). This suggests that resident kidney fibroblasts in miR-146b$^{-/-}$ females may not be induced to an excessively pro-fibrotic state by TGF-β and therefore this mechanism cannot fully account for the exacerbated renal fibrosis observed *in vivo*. Conversely, increasing the abundance of miR-146b-5p via exogenous pre-miR-146b delivery tended to reduce expression of the mesenchymal marker *Vim* and the fibrosis markers *Col1a1* and *Fn1* (Figure 11), especially in the presence of β-E_2. Intact females may be more susceptible to TGF-β-induced kidney damage than males in the absence of a protective upregulation of miR-146b-5p. Why estrogen promotes excessive renal fibrosis and pathology in the absence of miR-146b-5p is yet to be determined. The major finding of this study is, therefore, that these data support an important role of miR-146b-5p in mediating the protective benefit of estrogen in CKD in intact females. This may have important implications for our understanding and treatment of sex-specific presentations of CKD. There is great challenge in addressing the diverse and unique clinical needs of men and women with CKD. With the rising incidence of CKD co-morbidities and an aging population, CKD remains a significant health burden and an essential focus of basic research. We have generated a novel miR-146b$^{-/-}$ rat which provides a valuable tool to model sex-specific renocardiac pathology in the absence of a single miRNA. We have shown that the loss of miR-146b-5p alone can drive distinct pathological changes in male and female rats during the progression of CKD and CKD-mediated CVD. The data in this study

provide compelling rationale for future studies to investigate the molecular mechanism by which miR-146b-5p modulates CKD-related pathology, especially the potential role for miR-146b-5p in facilitating estrogen-dependent signaling and its link to the pro-fibrotic and pro-EMT TGF-β signaling cascade in CKD.

METHODS

Animal model

Animal protocols were approved by the MCW Institutional Animal Care and Use Committee. The *SD-Mir146b*^{em1Mcwi} (miR-146b$^{-/-}$) rat was developed using CRISPR/SpCas9 technology. A CRISPR guide RNA and SpCas9 targeting the sequence GCCTATGGAATTCA**GTTCTC***AGG* (protospacer adjacent motif italicized, miR-146b-5p seed sequence bolded and underlined) was successfully used to generate a 7-bp deletion mutation following pronuclear injection into Crl:SD rat embryos, resulting in a partial deletion of the miR-146b-5p seed sequence (Figure 1A). An outbred miR-146b$^{-/-}$ knockout model was maintained by continuous backcross to vendor Crl:SD at each generation with intercross of heterozygous offspring to generate miR-146b$^{-/-}$ and WT littermates. By maintaining an outbred colony and avoiding inbreeding, we mitigated potential unrecognized off-target effects of the CRISPR editing. This is the first reported line of global miR-146b-5p knockout rats.

Animals were maintained on a 0.4% NaCl diet (AIN-76A, Dyets, Inc., Bethlehem, PA) and provided water *ad libitum*. At 10 weeks of age, WT and miR-146b$^{-/-}$ males and females were given an anesthetic cocktail i.m. (ketamine, 50mg/kg; xylazine, 8mg/kg; and acepromazine, 5 mg/kg) and subjected to sham or 5/6Nx surgery using a surgical excision model.[11] To examine the contribution of gonadal hormones, a subset of females were ovariectomized (Ovx) during the same surgical procedure.

Longitudinal studies and cardiac phenotyping

Body weight was monitored and 24h urine volumes were collected in metabolic cages prior to echocardiography at weeks 0, 1, 3, 5, and 7 post-surgery (VIVID 7, GE, Chicago, IL).[11] LV pressure-volume relationships were measured with a Millar Mikro-Tip® pressure catheter on the MPVS Ultra system (Millar, Houston, TX).

Chronic blood pressure monitoring and renal phenotyping

To monitor chronic blood pressure in conscious animals, rats were instrumented with a PhysioTel™ HD-S10 single pressure transmitter (Data Sciences International, St. Paul, MN) in the peritoneal cavity. The catheter was advanced through the femoral artery into the abdominal aorta below the level of the renal arteries.[34] Blood pressure was recorded daily from 9:00a-12:00p and 3h averages were used for analysis. Data collection occurred for 3d of baseline blood pressures prior to surgical intervention and continued through 49d.

Urine and plasma electrolytes and creatinine were measured using the ABL800 Flex blood gas analyzer (Radiometer, Copenhagen, Denmark). $U_{malb}V$ was quantified with a fluorescent assay using Albumin Blue 580 dye (Molecular Probes, Eugene, OR) and a

fluorescent plate reader (FL600, Bio-Tek, Winooski, VT) and normalized to 24h urinary output.[35] CrCl [$(U_{Cr} \times V_{dt})/P_{Cr}$] and FE_{Na} [$(U_{Na} \times P_{Cr})/(P_{Na} \times U_{Cr}) \times 100$] were derived from plasma and urine concentrations and urine flow rate.[36]

Tissue collection and processing for qRT-PCR

Tissue were harvested under anesthesia at week 7 post-surgery. Kidney and heart tissue weights were normalized to body weight and frozen in liquid nitrogen or preserved in 10% formalin. Frozen tissues were pulverized and reserved for RNA extraction in TRIzol (ThermoFisher, Waltham, MA). Reverse transcription of total RNA was performed using the miScript II RT system (QIAGEN). Parallel quantification of pre-miR-146b and miR-146b-5p was performed by qRT-PCR utilizing the miScript SYBR® Green PCR system (QIAGEN). Quantification of fibrosis markers was performed using SYBR Green reagents with custom primer sequences listed in Supplementary Table S1. qRT-PCR of pri-miR-146b and EMT markers (*Vim* and *Cdh1*) was performed using pre-designed TaqMan assays (ThermoFisher). Relative abundance was quantified using the $2^{-\Delta\Delta Ct}$ method and abundance normalized to RNU6B or 18S rRNA.

Histological Analysis

Histological samples were processed by the CRI Histology Core at MCW. Tissues were sectioned at 4 μm for Masson's trichrome staining and 5 μm for ISH.[11, 37] Bright field micrographs were captured on a Nikon E-400 microscope. Fibrosis was quantified and reported as a percent of total area in the field of view.[38] We performed ISH for detection of miR-146b-5p in the kidney using a miRCURY LNA-enhanced digoxigenin-tagged miR-146b-5p probe (QIAGEN) with hybridization at 50°C and 100 nM probe.[37]

Western blot

Kidney tissue was processed for western blot analysis with quantification of Coomassie staining used to normalize protein load.[38] TGFB1 antibody (MAB240) was purchased from R&D Systems (Minneapolis, MN).

Pathway analysis of predicted miR-146b-5p targets

Predicted targets of miR-146b-5p (n=2,997; TargetScan[18]) were uploaded to IPA (QIAGEN) for identification of canonical pathways and toxicity lists (known clinical pathologies) enriched with miR-146b-5p targets.

Manipulation of miR-146b, TGF-β, and β–estradiol in NRK-49F

NRK-49F cells were maintained with Dulbecco's Modified Eagle Medium (Invitrogen, Waltham, MA) with 10% fetal bovine serum. Abundance of miR-146b-5p was manipulated *in vitro* by treating NRK-49F with either 133nM anti-miR-146b-5p (LNA™-modified oligonucleotides; Exiqon, Denmark) or 20nM exogenous pre-miR™-146b (Invitrogen), or equimolar concentrations of negative controls with scrambled sequence. Cell transfection was performed using Lipofectamine® 2000 (Invitrogen).[39] Following the 6h transfection, cells were treated with TGFB1 peptide (5ng/ml) and/or β-estradiol (10μM). Cells were harvested in TRIzol after 48h for RNA extraction and qRT-PCR.

Statistical Analysis

All data shown as mean ± SEM and analyzed using multiple-group ANOVA (with repeated measures where appropriate) with the Holm-Sidak post-hoc test. $p<0.05$ considered statistically significant.

Supplementary Material

Refer to Web version on PubMed Central for supplementary material.

ACKNOWLEDGEMENTS

The authors extend sincere thanks to Dr. David Mattson for expert consultation on biochemical analysis, and the Biochemical Core Laboratory for their technical assistance; both from the Department of Physiology, MCW (Milwaukee, WI).

Funding: This work was supported by grants from the National Institutes of Health [8UL1TR000055, R01HL128332] and American Heart Association [13SDG17100095].

REFERENCES

1. Centers for Disease Control and Prevention. Chronic Kidney Disease Surveillance System - United States. Website. http://nccd.cdc.gov/CKD.
2. Jha V, Garcia-Garcia G, Iseki K, et al. Chronic kidney disease: global dimension and perspectives. Lancet 2013; 382: 260–272. [PubMed: 23727169]
3. Gansevoort RT, Correa-Rotter R, Hemmelgarn BR, et al. Chronic kidney disease and cardiovascular risk: epidemiology, mechanisms, and prevention. Lancet 2013; 382: 339–352. [PubMed: 23727170]
4. Herzog CA, Asinger RW, Berger AK, et al. Cardiovascular disease in chronic kidney disease. A clinical update from Kidney Disease: Improving Global Outcomes (KDIGO). Kidney Int 2011; 80: 572–586. [PubMed: 21750584]
5. Neugarten J, Acharya A, Silbiger SR. Effect of gender on the progression of nondiabetic renal disease: a meta-analysis. J Am Soc Nephrol 2000; 11: 319–329. [PubMed: 10665939]
6. Carrero JJ, Hecking M, Chesnaye NC, et al. Sex and gender disparities in the epidemiology and outcomes of chronic kidney disease. Nat Rev Nephrol 2018; 14: 151–164. [PubMed: 29355169]
7. United States Renal Data System. 2017 USRDS annual data report: Epidemiology of kidney disease in the United States. National Institutes of Health, National Institute of Diabetes and Digestive and Kidney Diseases, Bethesda, MD, 2017.
8. Dubey RK, Jackson EK. Estrogen-induced cardiorenal protection: potential cellular, biochemical, and molecular mechanisms. Am J Physiol Renal Physiol 2001; 280: F365–388. [PubMed: 11181399]
9. Stehman-Breen CO, Gillen D, Gipson D. Prescription of hormone replacement therapy in postmenopausal women with renal failure. Kidney Int 1999; 56: 2243–2247. [PubMed: 10594801]
10. Krol J, Loedige I, Filipowicz W. The widespread regulation of microRNA biogenesis, function and decay. Nat Rev Genet 2010; 11: 597–610. [PubMed: 20661255]
11. Chuppa S, Liang M, Liu P, et al. MicroRNA-21 regulates peroxisome proliferator-activated receptor alpha, a molecular mechanism of cardiac pathology in Cardiorenal Syndrome Type 4. Kidney Int 2017.
12. Liu Y, Usa K, Wang F, et al. MicroRNA-214-3p in the Kidney Contributes to the Development of Hypertension. J Am Soc Nephrol 2018.
13. Baker MA, Davis SJ, Liu P, et al. Tissue-Specific MicroRNA Expression Patterns in Four Types of Kidney Disease. J Am Soc Nephrol 2017; 28: 2985–2992. [PubMed: 28663230]
14. Pellegrini KL, Gerlach CV, Craciun FL, et al. Application of small RNA sequencing to identify microRNAs in acute kidney injury and fibrosis. Toxicol Appl Pharmacol 2016; 312: 42–52. [PubMed: 26707937]

15. Zawada AM, Rogacev KS, Muller S, et al. Massive analysis of cDNA Ends (MACE) and miRNA expression profiling identifies proatherogenic pathways in chronic kidney disease. Epigenetics 2014; 9: 161–172. [PubMed: 24184689]
16. Paterson MR, Kriegel AJ. MiR-146a/b: a family with shared seeds and different roots. Physiol Genomics 2017; 49: 243–252. [PubMed: 28213571]
17. Chen Y, Heiman ML. Increased weight gain after ovariectomy is not a consequence of leptin resistance. Am J Physiol Endocrinol Metab 2001; 280: E315–322. [PubMed: 11158936]
18. Agarwal V, Bell GW, Nam JW, et al. Predicting effective microRNA target sites in mammalian mRNAs. Elife 2015; 4.
19. Lemos CC, Tovar AM, Guimaraes MA, et al. Effect of castration on renal glycosaminoglycans and their urinary excretion in male and female rats with chronic renal failure. Braz J Med Biol Res 2013; 46: 567–573. [PubMed: 23970064]
20. Lu H, Lei X, Klaassen C. Gender differences in renal nuclear receptors and aryl hydrocarbon receptor in 5/6 nephrectomized rats. Kidney Int 2006; 70: 1920–1928. [PubMed: 16985511]
21. Griffin KA. Hypertensive Kidney Injury and the Progression of Chronic Kidney Disease. Hypertension 2017; 70: 687–694. [PubMed: 28760941]
22. Jafar TH, Schmid CH, Stark PC, et al. The rate of progression of renal disease may not be slower in women compared with men: a patient-level meta-analysis. Nephrol Dial Transplant 2003; 18: 2047–2053. [PubMed: 13679479]
23. O'Hare AM, Choi AI, Bertenthal D, et al. Age affects outcomes in chronic kidney disease. J Am Soc Nephrol 2007; 18: 2758–2765. [PubMed: 17855638]
24. Reckelhoff JF, Fortepiani LA. Novel mechanisms responsible for postmenopausal hypertension. Hypertension 2004; 43: 918–923. [PubMed: 15023933]
25. Hinojosa-Laborde C, Lange DL, Haywood JR. Role of female sex hormones in the development and reversal of dahl hypertension. Hypertension 2000; 35: 484–489. [PubMed: 10642346]
26. Antus B, Hamar P, Kokeny G, et al. Estradiol is nephroprotective in the rat remnant kidney. Nephrol Dial Transplant 2003; 18: 54–61. [PubMed: 12480960]
27. Schunkert H, Danser AH, Hense HW, et al. Effects of estrogen replacement therapy on the renin-angiotensin system in postmenopausal women. Circulation 1997; 95: 39–45. [PubMed: 8994414]
28. Liang M MicroRNA: a new entrance to the broad paradigm of systems molecular medicine. Physiol Genomics 2009; 38: 113–115. [PubMed: 19470802]
29. Bottinger EP, Bitzer M. TGF-beta signaling in renal disease. J Am Soc Nephrol 2002; 13: 2600–2610. [PubMed: 12239251]
30. Loeffler I, Wolf G. Transforming growth factor-beta and the progression of renal disease. Nephrol Dial Transplant 2014; 29 Suppl 1: i37–i45. [PubMed: 24030832]
31. Gomez-Garre D, Ruiz-Ortega M, Ortego M, et al. Effects and interactions of endothelin-1 and angiotensin II on matrix protein expression and synthesis and mesangial cell growth. Hypertension 1996; 27: 885–892. [PubMed: 8613264]
32. Kagami S, Border WA, Miller DE, et al. Angiotensin II stimulates extracellular matrix protein synthesis through induction of transforming growth factor-beta expression in rat glomerular mesangial cells. J Clin Invest 1994; 93: 2431–2437. [PubMed: 8200978]
33. Lee JM, Dedhar S, Kalluri R, et al. The epithelial-mesenchymal transition: new insights in signaling, development, and disease. J Cell Biol 2006; 172: 973–981. [PubMed: 16567498]
34. Griffin KA, Picken M, Bidani AK. Radiotelemetric BP monitoring, antihypertensives and glomeruloprotection in remnant kidney model. Kidney Int 1994; 46: 1010–1018. [PubMed: 7861695]
35. De Miguel C, Das S, Lund H, et al. T lymphocytes mediate hypertension and kidney damage in Dahl salt-sensitive rats. Am J Physiol Regul Integr Comp Physiol 2010; 298: R1136–1142. [PubMed: 20147611]
36. Espinel CH. The FENa test. Use in the differential diagnosis of acute renal failure. JAMA 1976; 236: 579–581. [PubMed: 947239]
37. Kriegel AJ, Liang M. MicroRNA in situ hybridization for formalin fixed kidney tissues. J Vis Exp 2013.

38. Kriegel AJ, Liu Y, Cohen B, et al. MiR-382 targeting of kallikrein 5 contributes to renal inner medullary interstitial fibrosis. Physiol Genomics 2012; 44: 259–267. [PubMed: 22202692]

39. Nasci VL, Chuppa S, Griswold L, et al. miR-21-5p regulates mitochondrial respiration and lipid content in H9C2 cells. Am J Physiol Heart Circ Physiol 2019; 316: H710–H721. [PubMed: 30657727]

TRANSLATIONAL STATEMENT

Within precision medicine initiatives, special attention is given to divergent clinical presentations of CKD in men and women, and how advancement of clinical care relies upon a better understanding of sex-specific pathologies. This study proposes a novel role for miR-146b-5p in mediating the protective benefit of estrogen in CKD. We show loss of miR-146b-5p elicits drastic changes in kidney pathology in a rodent model of CKD – changes that are starkly sex-specific. This work has potential to uncover an exciting path towards better management of CKD and CKD-related cardiovascular disease (CVD) by identifying novel miR-146b-5p-regulated disease signaling pathways.

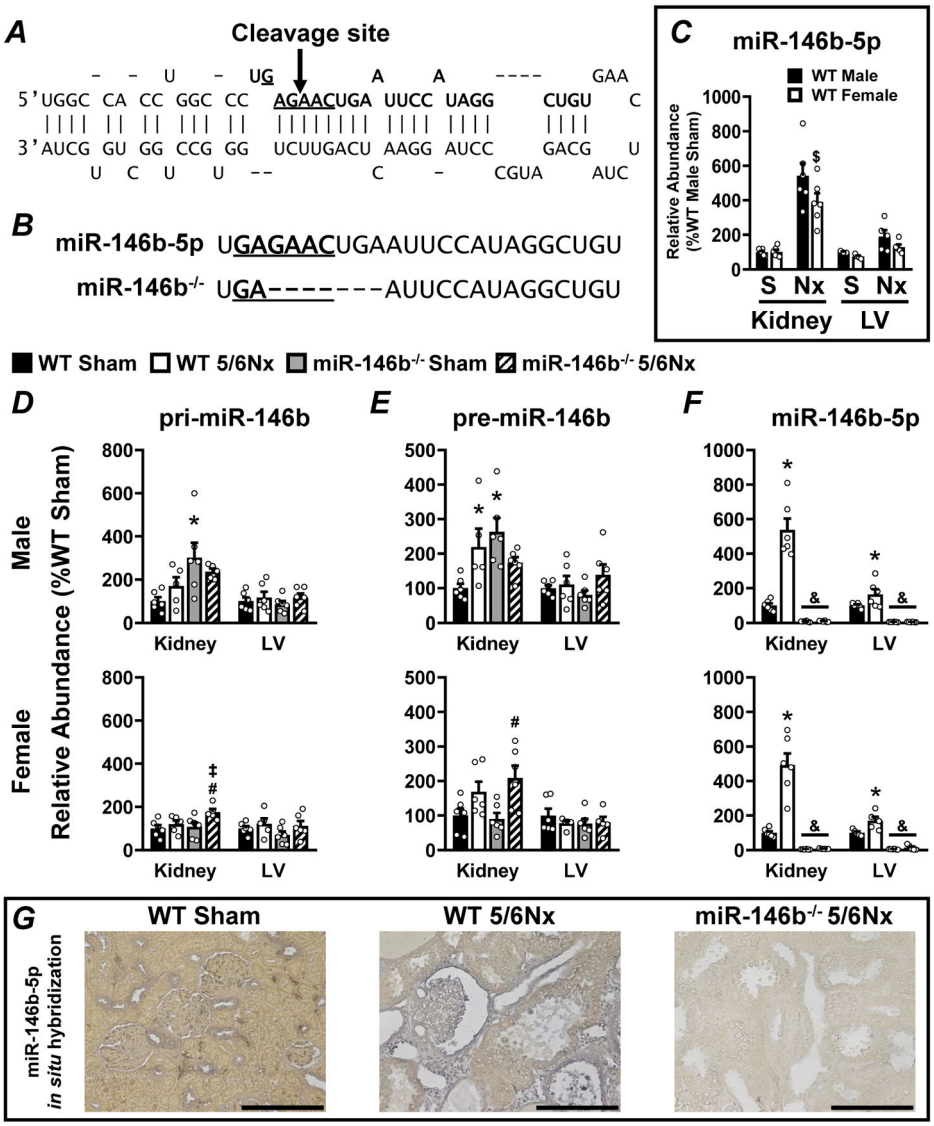

Figure 1: Efficient knockout of miR-146b-5p in SD rats in both the kidney and the LV in males and females.

CRISPR guide RNAs were designed to target within the seed sequence of *Mir146b*. (A) A diagram representing the stem-loop sequence of *Mir146b* highlights the seed sequence (underlined base pairs) of the mature miR-146b-5p sequence (base pairs in bold typeface). CRISPR-Cas9 targeting to this region resulted in a cleavage site within the seed sequence indicated by the arrow. (B) CRISPR-Cas9-mediated cleavage of Mir146b resulted in a 7-bp deletion overlapping the seed sequence of miR-146b-5p, indicated by dashed lines in bottom sequence. *Mir146b* gene products were characterized by qRT-PCR in both kidney and LV tissue: comparing (C) basal levels of miR-146b-5p in male vs. female WT, and the abundance of (D) primary Mir-146b transcript (pri-miR-146b), (E) the intermediate precursor (pre-miR-146b), and (F) the mature, bioactive, miR-146-5p in each experimental group. (G) ISH of miR-146b-5p in kidney tissue; representative images shown for WT sham, WT 5/6Nx and miR-146b$^{-/-}$ 5/6Nx. All data presented as mean ± SEM, n = 5-6/group; $

p<0.05 WT female vs. WT male; * p<0.05 WT 5/6Nx vs. WT Sham; # p<0.05 miR-146b $^{-/-}$ 5/6Nx vs. miR-146b$^{-/-}$ Sham; ‡ p<0.05 miR-146b$^{-/-}$ 5/6Nx vs. WT 5/6Nx; & p<0.05 miR-146b$^{-/-}$ vs. WT within all groups.

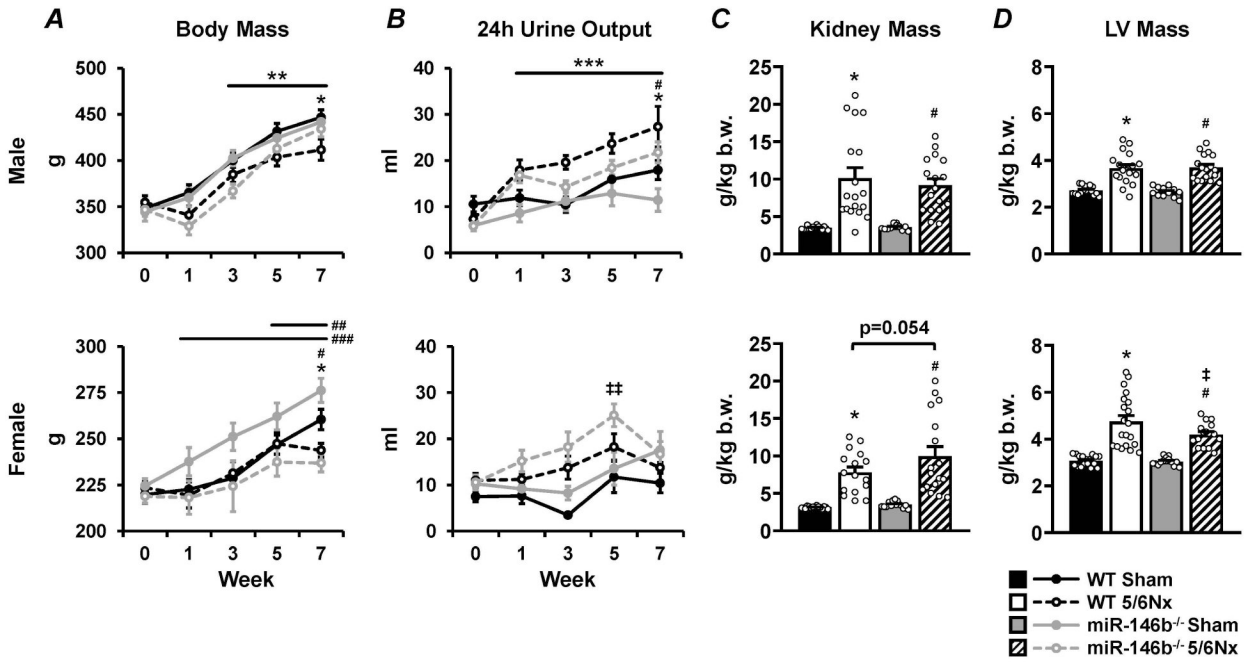

Figure 2: Growth curves, urinary output, and renal and cardiac hypertrophy in WT and miR-146b$^{-/-}$ rats following 5/6Nx.

(A) Body mass and (B) 24h urinary output over the 7-week study, along with (C) renal hypertrophy and (D) cardiac hypertrophy at the end of the study reported for males (top row) and females (bottom row). All data presented as mean ± SEM, n = 7-20/group; * p<0.05 WT 5/6Nx vs. WT Sham; # p<0.05 miR-146b$^{-/-}$ 5/6Nx vs. miR-146b$^{-/-}$ Sham; ‡ p<0.05 miR-146b$^{-/-}$ 5/6Nx vs. WT 5/6Nx; ** p<0.05 vs. Week 0 across all groups; *** p<0.05 5/6Nx vs. Sham within each genotype; ## p<0.05 vs Week 0 for WT 5/6Nx; ### p<0.05 vs. Week 0 within Sham groups, both WT and miR-146b$^{-/-}$; ‡‡ p<0.05 vs. Week 0 for miR-146b$^{-/-}$ 5/6Nx at indicated time point.

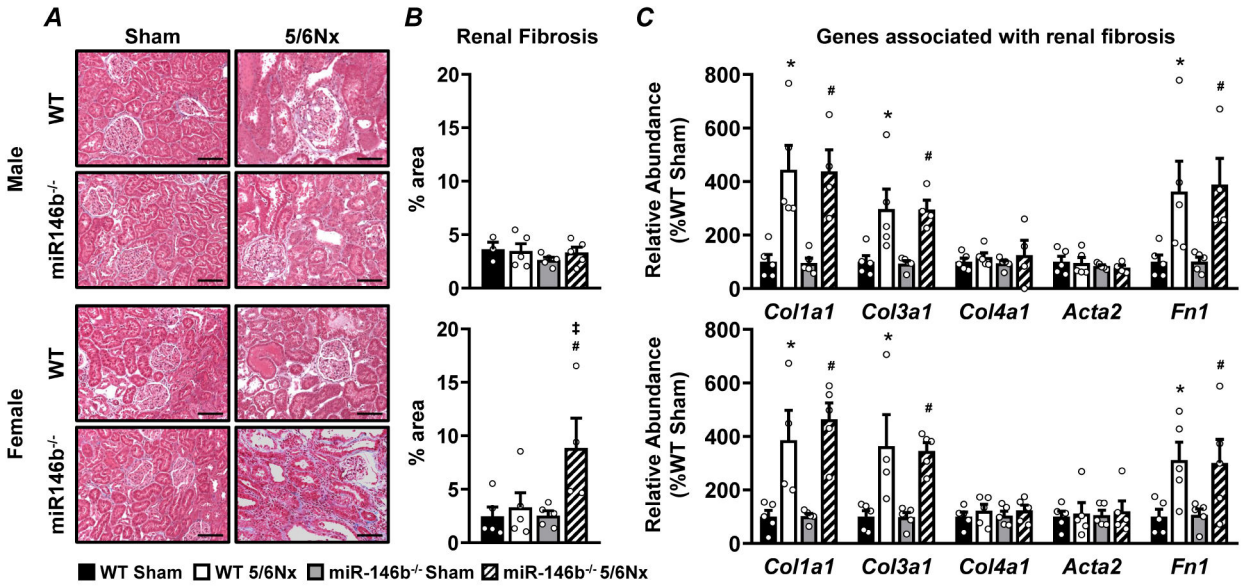

Figure 3: Sex-specific renal fibrosis in females exacerbated by miR-146b-5p knockout^{-}.

(A) Masson's trichrome stain of kidney tissue from male (top) and female (bottom) groups, organized by quadrant as indicated with (B) fibrotic region (blue stain) quantified as % of total area. (C) Transcript abundance of genes associated with renal fibrosis were measured by qRT-PCR. All data presented as mean ± SEM, n = 3-5/group; * p<0.05 WT 5/6Nx vs. WT Sham; # p<0.05 miR-146b$^{-/-}$ 5/6Nx vs. miR-146b$^{-/-}$ Sham. Scale bar = 100μm.

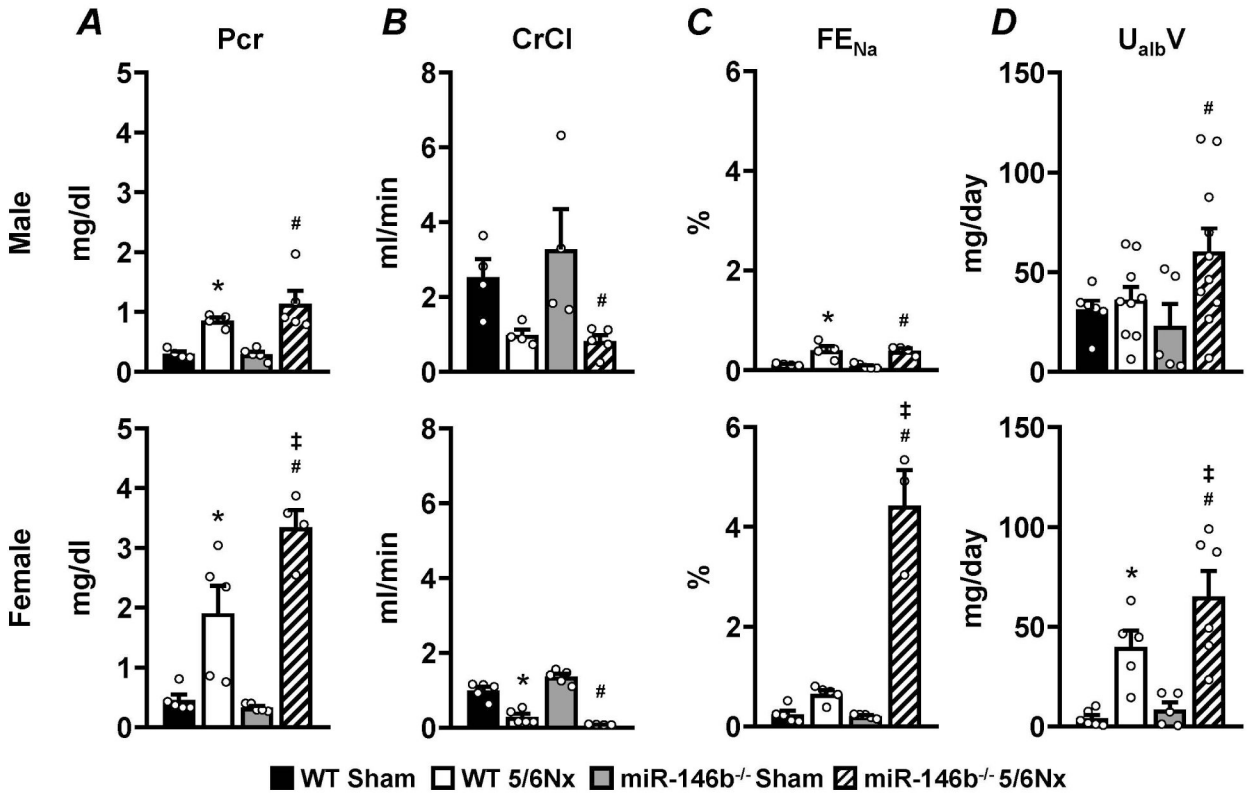

Figure 4: Urine and plasma analysis reveals sex-specific renal dysfunction.

To assess renal function, urine and plasma samples from week 7 were analyzed for (A) plasma creatinine concentration, (B) CrCl, (C) FE_{Na}, and (D) $U_{malb}V$. All data presented as mean ± SEM, n = 3-5/group; * $p<0.05$ WT 5/6Nx vs. WT Sham; # $p<0.05$ miR-146b $^{-/-}$ 5/6Nx vs. miR-146b$^{-/-}$ Sham; ‡ $p<0.05$ vs. WT 5/6Nx.

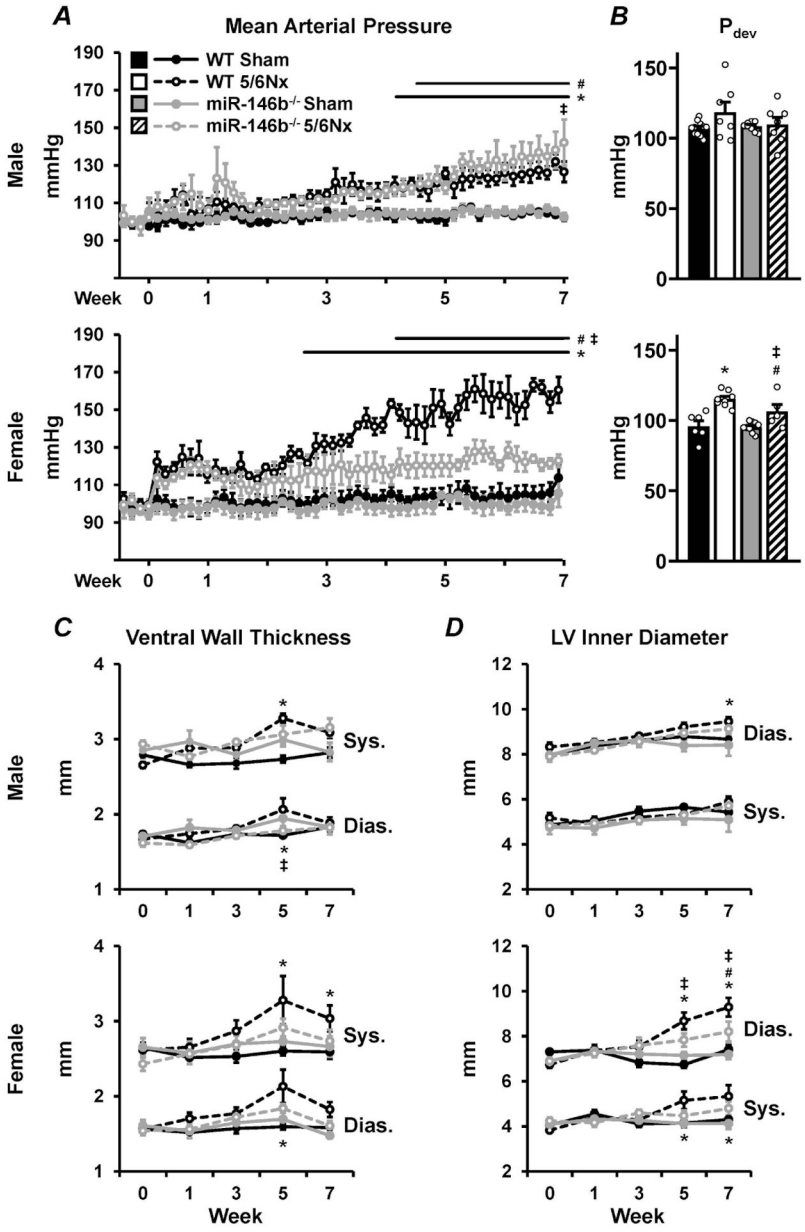

Figure 5: Chronic blood pressure monitoring reveals sex-specific divergence of cardiovascular pathologies.

Chronic radiotelemetry implants used to measure (A) conscious ambulatory blood pressure in males (top) and females (bottom), here reported as MAP. (B) LV developed pressure was measured acutely at week 7 with the use of a Millar pressure catheter. LV structure was measured using echocardiography to monitor (C) ventral wall thickness and (D) LV chamber diameter throughout the cardiac cycle. All data presented as mean ± SEM, n = 3-15/group; * $p<0.05$ WT 5/6Nx vs. WT Sham; # $p<0.05$ miR-146b$^{-/-}$ 5/6Nx vs. miR-146b$^{-/-}$ Sham; ‡ $p<0.05$ miR-146b$^{-/-}$ 5/6Nx vs. WT 5/6Nx; & $p<0.05$ miR-146b$^{-/-}$ 5/6Nx vs. WT 5/6Nx.

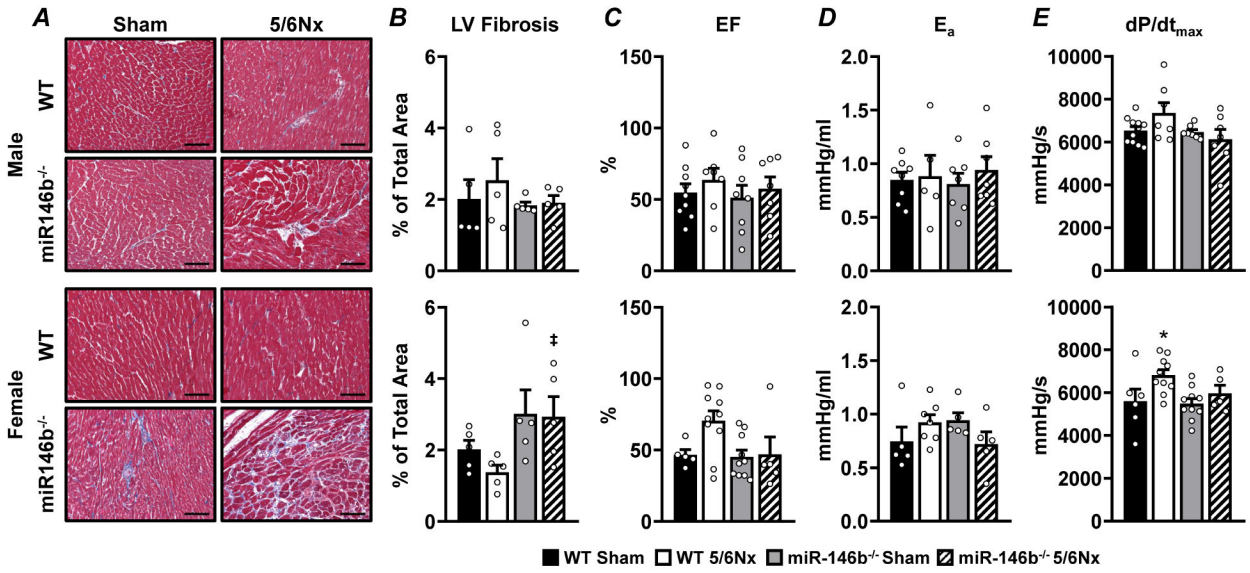

Figure 6: Rats exhibit mild cardiovascular phenotypes, regardless of sex or genotype, following 5/6Nx.

(A) Masson's trichrome stain of LV tissue from male (top) and female (bottom) groups, organized by quadrant as indicated with (B) fibrotic region (blue stain) quantified as % of total area. To assess cardiovascular function at week 7, a Millar pressure catheter was used to measure (C) Ejection fraction, (D) arterial elastance, and (E) dP/dt_{max}, a measure of LV contractility. All data presented as mean ± SEM, n = 3-11/group; *p<0.05 WT 5/6Nx vs. WT Sham; ‡ p<0.05 miR-146b$^{-/-}$ 5/6Nx vs. WT 5/6Nx. Scale bar = 100μm.

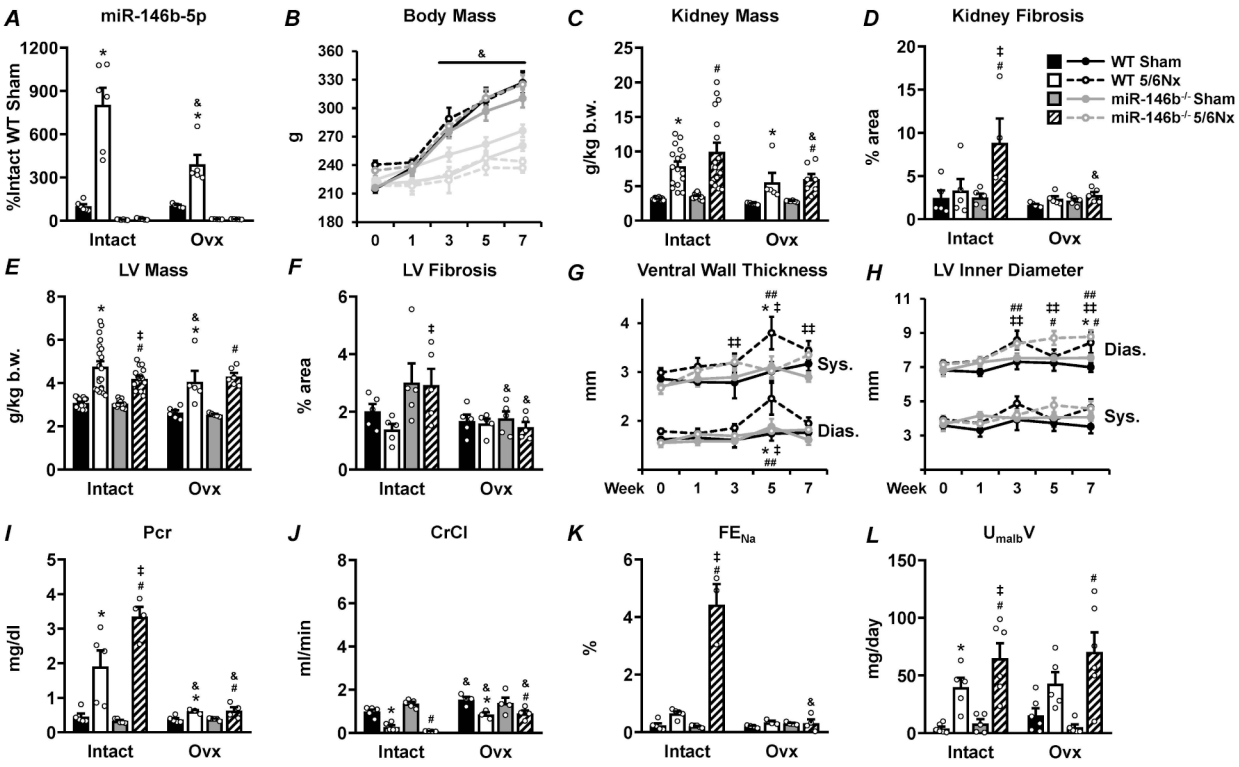

Figure 7: Ovx significantly attenuates renal pathology and abolishes genotypic differences after 5/6Nx.

Complete ovariectomy was performed on a subset of females at the time of the 5/6Nx or sham surgery. Light gray bars or lines represent data from intact females which are paired with their corresponding Ovx counterparts. (A) Relative abundance of miR-146b-5p and gross phenotypes were assessed; including (B) body mass, (C) renal hypertrophy, (D) renal fibrosis, (E) cardiac hypertrophy, and (F) cardiac fibrosis. Structural changes in the LV were assessed by echocardiography, including (G) ventral wall thickness and (H) chamber diameter. Renal function was assessed by urine and plasma analysis of (I) plasma creatinine, (J) CrCl, (K) FE_{Na} and (L) $U_{malb}V$. All data presented as mean ± SEM, n = 3-15/group; * p<0.05 WT 5/6Nx vs. WT Sham; # p<0.05 vs. miR-146b$^{-/-}$ 5/6Nx vs. miR-146b$^{-/-}$ Sham; ‡ p<0.05 miR-146b$^{-/-}$ 5/6Nx vs. WT 5/6Nx; ## p<0.05 vs Week 0 for WT 5/6Nx ; ‡‡ p<0.05 vs. Week 0 for miR-146b$^{-/-}$ 5/6Nx; & p<0.05 Ovx vs. Intact within indicated groups.

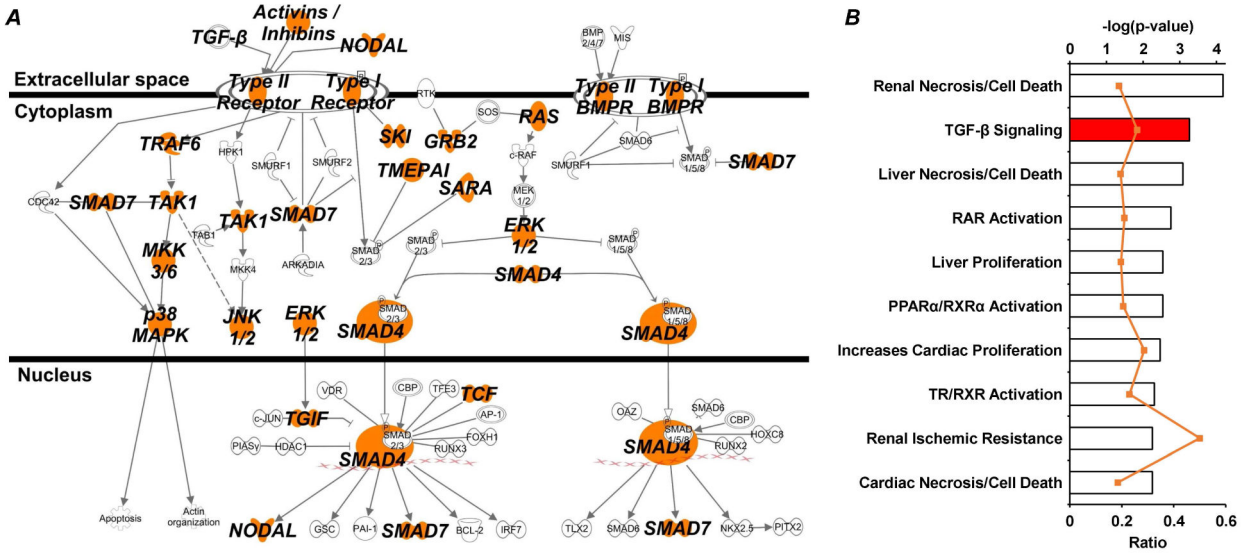

Figure 8: Pathway analysis of miR-146b-5p targets suggests important role for TGF-β signaling.

Predicted targets of miR-146b-5p were analyzed using IPA software to identify over-represented canonical pathways and provide strong rationale for further investigation. Both the (A) canonical TGF-β signaling pathway and the (B) TGF-β toxicity list (i.e. biological functions associated with pathological outcomes) had a disproportionate representation of miR-146b-5p targets. (A) Each node within the canonical TGF-β pathway containing a predicted target is highlighted orange. (B) The top axis (bar graph) represents p-value associated with the toxicity list based on target representation and the bottom axis (orange line) represents the ratio of molecules within the given toxicity list that are miR-146b-5p targets.

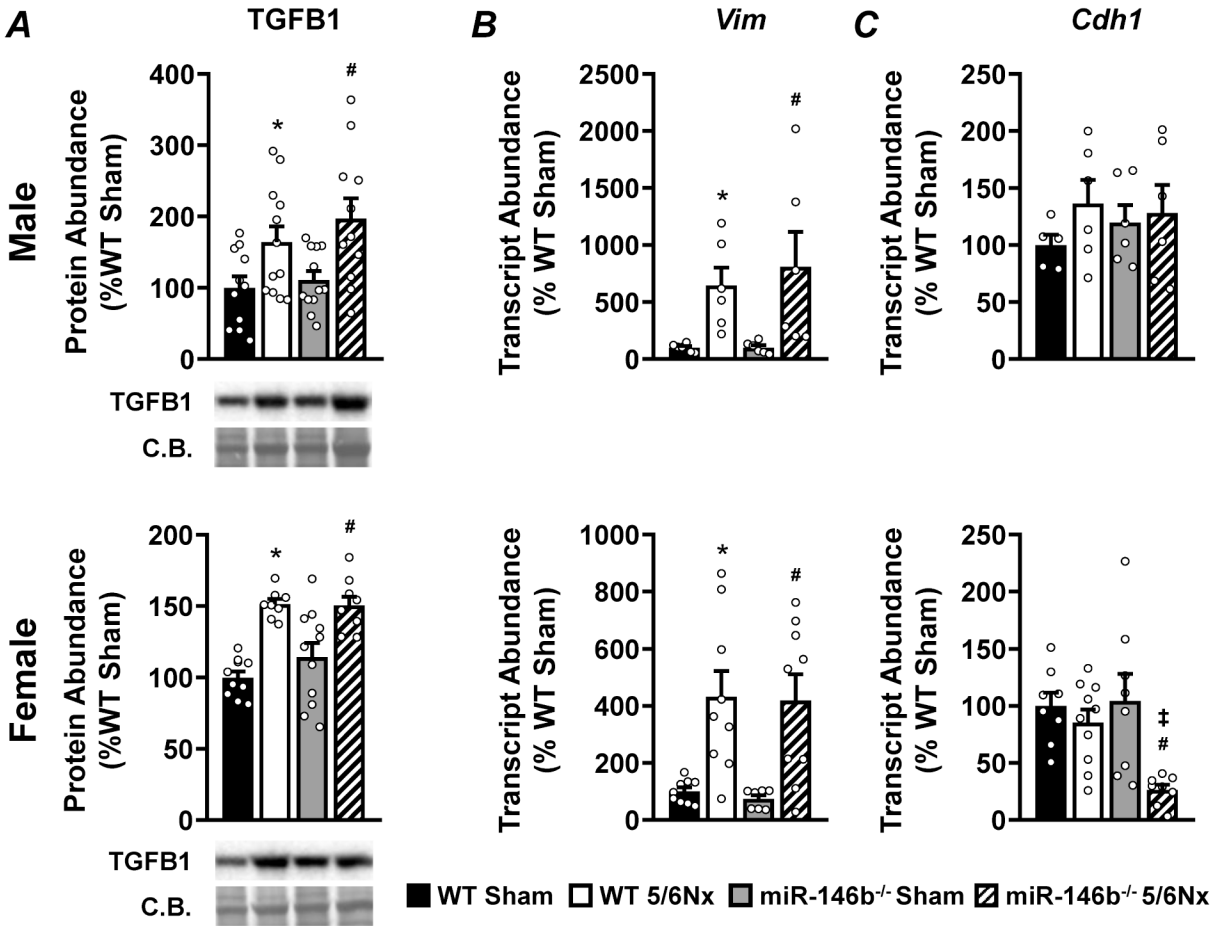

Figure 9: 5/6Nx induces TGFB1 expression and a mesenchymal phenotype; epithelial phenotype may be lost in miR-146b$^{-/-}$ 5/6Nx females.

(A) Western blot analysis of TGFB1 abundance. qRT-PCR analysis of (B) the mesenchymal marker *Vim* and (C) the epithelial marker *Cdh1*. All data presented as mean ± SEM, n = 6-12/group; * p<0.05 WT 5/6Nx vs. WT Sham; # p<0.05 miR-146b$^{-/-}$ 5/6Nx vs. miR-146b$^{-/-}$ Sham; ‡ p<0.05 miR-146b$^{-/-}$ 5/6Nx vs. WT 5/6Nx.

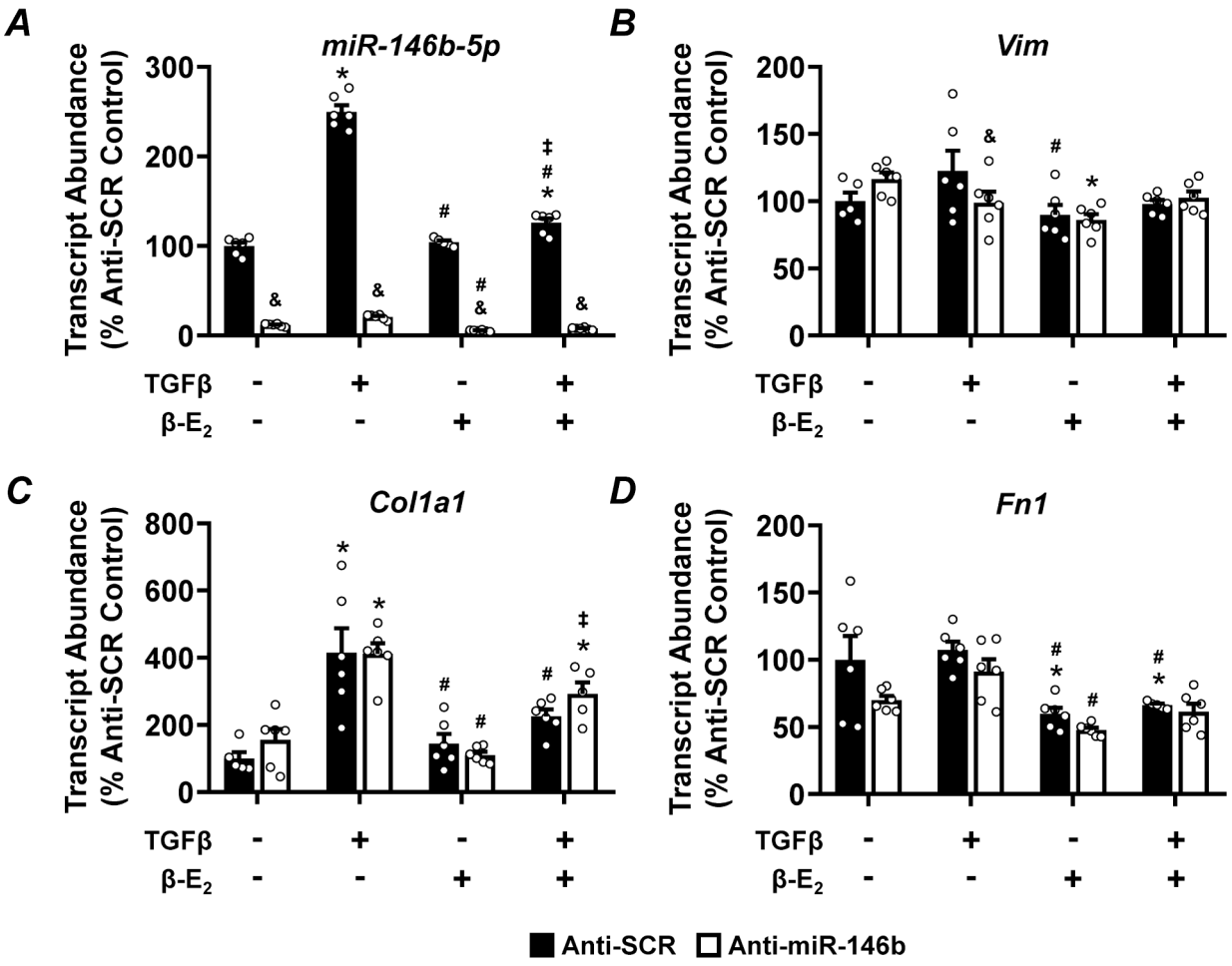

Figure 10: Anti-miR-146b-5p treatment of NRK-49F cells does not augment expression of pro-fibrotic markers.

qRT-PCR analysis of (A) miR-146b-5p abundance, (B) the mesenchymal marker *Vim* and the pro-fibrotic markers (C) *Col1a1*, and (D) *Fn1* from NRK-49F cells treated with anti-miR-146b-5p. All data presented as mean ± SEM, n = 6/group; * $p<0.05$ vs. control within group; # $p<0.05$ vs. TGF-β only, within group; ‡ $p<0.05$ vs. β-E_2 only, within group; & $p<0.05$ anti-miR-146b vs. anti-SCR between indicated groups.

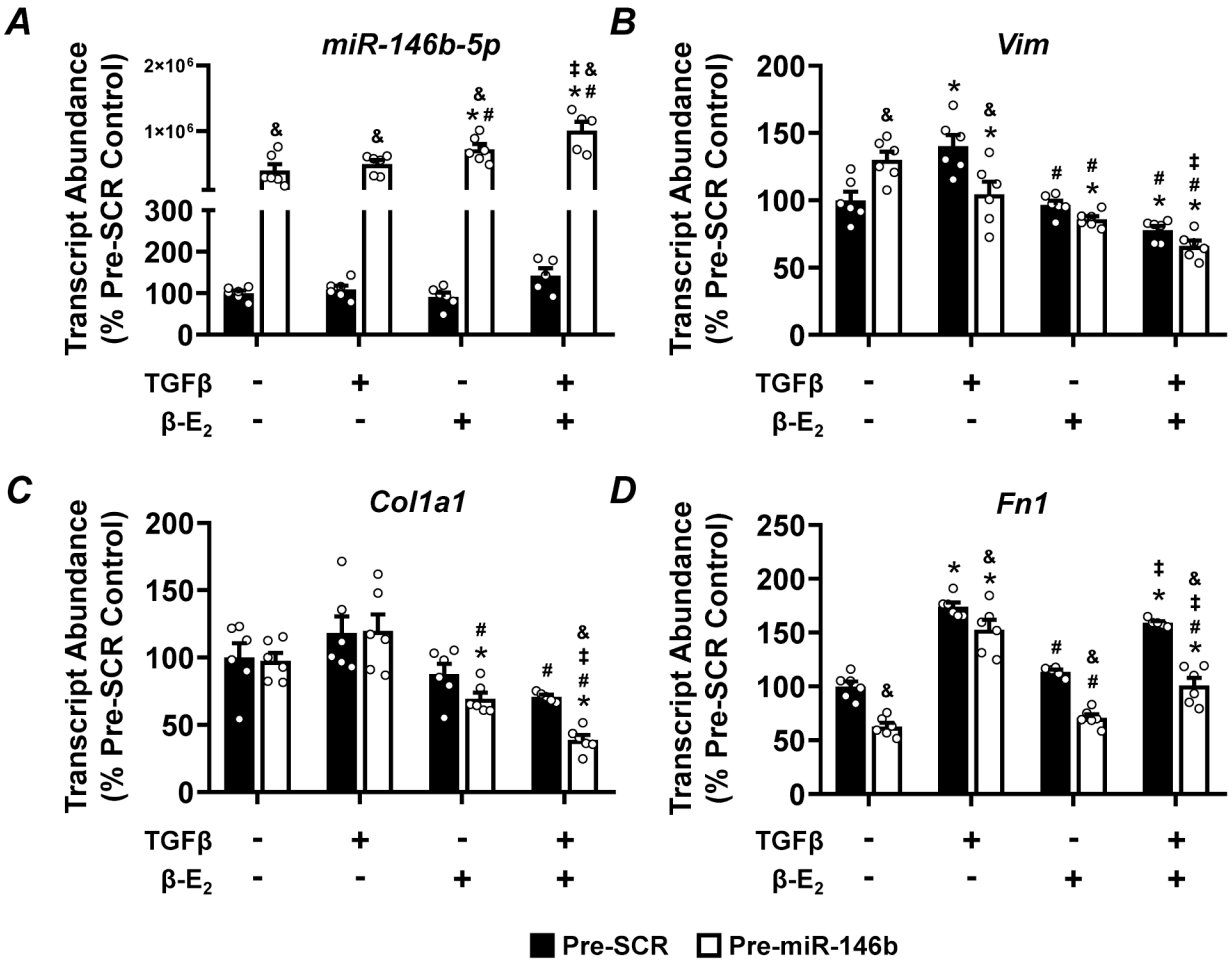

Figure 11: Pre-miR-146b treatment of NRK-49F cells may blunt expression of pro-fibrotic markers.

qRT-PCR analysis of (A) miR-146b-5p abundance, (B) the mesenchymal marker *Vim* and the pro-fibrotic markers (C) *Col1a1*, and (D) *Fn1* from NRK-49F cells treated with pre-miR-146b. All data presented as mean ± SEM, n = 6/group; * $p<0.05$ vs. control within group; # $p<0.05$ vs. TGF-β only, within group; ‡ $p<0.05$ vs. β-E_2 only, within group; & $p<0.05$ pre-miR-146b vs. anti-SCR between indicated groups.